RSC Advances

PAPER

View Article Online
View Journal | View Issue

Cite this: *RSC Adv.*, 2025, **15**, 14756

Comprehensive analysis of experimental conditions in plasma–liquid interaction for the efficient removal of methylene blue†

Duc Trung Vo,[ab] Nga Thi Dinh, *[c] Tam Huynh Thanh Le,[b] Duc Trung Nguyen,[b] Lan Thi Phan,[d] Hoang Tung Do,[e] Young Sun Mok *[a] and Duc Ba Nguyen *[fg]

A comprehensive investigation of the input parameters in a plasma–liquid interaction (PLI) for the removal of methylene blue (MB) in artificial wastewater was conducted using a cold atmospheric pressure Ar plasma jet (jet temperature ≤ 40 °C). The Ar plasma jet was generated by a gliding arc configuration and driven with a 50 Hz AC high voltage. The effects of key parameters on MB removal efficiency were systematically examined, including stirring solution, distance from the plasma jet source to the liquid surface, interaction time, initial MB concentration, and Ar flow rate. These results indicate that increasing the Ar flow rate, treatment time, and stirring solution improved the MB removal efficiency. In contrast, the efficiency decreased with distance and the initial MB solution. To evaluate the magnitude of these factors, a quadratic equation was developed to predict MB removal efficiency, demonstrating good agreement with the experimental data. Consequently, the relative importance of the factors based on first-order coefficients was determined as follows: treatment time > Ar flow rate > initial MB concentration > distance > stirring solution. These findings provide valuable insights for optimizing the plasma configuration and operating conditions for efficient MB removal *via* PLI treatment. Remarkably, 99% of MB degradation in the feed (20 mg L^{-1}) was achieved within 50 minutes of treatment, with an energy efficiency of 82.76 mg MB per kW per h, corresponding to 241.67 kW h m^{-3} for an initial MB of 20 mg L^{-1}. This process is environmentally friendly owing to its low electrical energy consumption and the fact that no chemicals are used.

Received 13th February 2025
Accepted 22nd April 2025

DOI: 10.1039/d5ra01066g

rsc.li/rsc-advances

1 Introduction

The more modern human society is, the more diverse fashion needs there are in terms of designs, materials, and colors. Consequently, the textile and dyeing industry is growing rapidly around the world.[1] To create a dyed textile product, raw materials must go through many stages, such as knitting, washing, blenching, coloring, laundering, and completing. During these processes, a huge amount of water is consumed, and an equal volume of wastewater is generated.[2] Methylene blue (MB) is considered one of the most common colorants in the textile industry. The MB formula is $C_{16}H_{18}ClN_3S$ (the weight of a molecule is 319.85 g mol^{-1}); it is a cationic dye and heterocyclic aromatic compound.[3] A huge amount of MB is used in the cosmetics, textiles, leather, and pharmaceutical industries, and a large volume of wastewater containing this dye is discharged into the environment.[1] It penetrates water bodies, causing pollution of surface water and groundwater if not thoroughly treated. Many publications have confirmed that MB is the cause of several diseases as they are teratogenic, carcinogenic, and embryotoxic for rats and fish.[4] MB poisoning in humans was also described through manifestations such as sickness, high blood pressure, anemia, and intellectual and skin injuries.[3] It was reported that a minimum dosage of 5 mg MB per kg might cause fatal serotonin toxicity in humans or be a threat to fauna in aquatic ecosystems.[5] Therefore, MB dye removal from wastewater is crucial for sustainable development.[6,7]

Research, development, and application of innovative technologies for removing MB in water have increasingly focused on addressing environmental issues related to this colorant.[4] To date, the basic approaches for treating organic matter in

[a]*Department of Chemical Engineering, Jeju National University, Jeju 63243, Republic of Korea. E-mail: smokie@jejunu.ac.kr*

[b]*Research Institute for Sustainable Development, Ho Chi Minh City University of Natural Resources and Environment, Hochiminh City, Vietnam*

[c]*Institute of Environmental Science, Engineering and Management, Industrial University of Ho Chi Minh City, Go Vap, Ho Chi Minh City, Vietnam. E-mail: dinhthinga@iuh.edu.vn*

[d]*Faculty of Electronic Engineering I, Posts and Telecommunications Institute of Technology, Hanoi, Vietnam*

[e]*Institute of Physics, Vietnam Academy of Science and Technology, 10 Dao Tan, Ba Dinh, Hanoi, Vietnam*

[f]*Institute of Theoretical and Applied Research, Duy Tan University, Hanoi 100000, Vietnam. E-mail: band@plasma.ac.vn*

[g]*Faculty of Environmental and Chemical Engineering, Duy Tan University, Danang 550000, Vietnam*

† Electronic supplementary information (ESI) available: Experimental data for Box–Behnken design; result of model analysis. See DOI: https://doi.org/10.1039/d5ra01066g

wastewater have been physical, chemical, biological, or combined processes.[8–12] The advantages of physical approaches are that they are simple to design, are easy to operate, have low treatment costs, and generate limited sludge.[13,14] However, this method may have drawbacks, such as slow applicability and incomplete treatment consequences of generating toxic by-products.[15] In other treatment directions, physicochemical pathways commonly used for effective dye removal include coagulation–flocculation, electrochemical, and advanced oxidation processes. However, chemical processes also have many limitations, such as high costs, large volumes of hazardous sludge generated after treatment, high electrical energy requirements, and the requirement for proper equipment.[16–18] Biological treatment is often applied as a secondary treatment stage for textile wastewater following physical and chemical treatment. This process helps improve treatment efficiency and reduce costs per unit volume of wastewater. However, the generation of large amounts of biomass sludge requiring further treatment and greenhouse gas emissions in anaerobic wastewater treatment are problems that contribute to global warming.[19–23] Moreover, biological methods are economically feasible;[24] however, these approaches are less effective and consequently require a lengthy processing time.[25]

Although conventional wastewater treatment methods, such as physical, physicochemical, and biological processes, face limitations, such as slow kinetics, sludge generation, high costs, or the generation of toxic by-products, atmosphere-pressure non-thermal plasma (NTP) has emerged as a highly efficient and environmentally superior alternative, aligning perfectly with the growing focus on sustainable technologies. Indeed, regarding environmentally friendly technology, NTP has emerged as a highly efficient and environmentally compatible tool for activating advanced oxidation processes (AOPs).[26–28] The scientific community has shown significant interest in this technology.[29–31] The exceptional efficiency of NTP is attributed to the generation of numerous reactive oxygen species (RON), including $O^{\bullet}$, O_2^*, O_2^-, $^{\bullet}OH$, H_2O_2, and O_3.[32–34] These highly reactive species effectively degrade and mineralize organic pollutants through direct bond breaking, often achieving significantly faster rates and crucially avoiding the hazardous by-products commonly associated with chemical treatment methods. Furthermore, NTP's synergistic combination of the chemical and physical effects, including localized heat and UV photons, offers a comprehensive and practical approach to treating dye-contaminated wastewater, effectively overcoming many of the key drawbacks inherent in traditional techniques and positioning it as a greener solution.

Dye-contaminated removal by NTP treatment is an advanced oxidation process that presents effectiveness and green technology in dye treatment.[35–40] Aloui *et al.*[37] showed a method for degrading MB by pulsed nanosecond discharge in water with Ar–O_2 gaseous plasma bubbles, which are generated by a novel one-electrode setup (a needle-to-plate configuration) and a four-electrode setup (four needle-to-wire configuration). The degradation of MB was obtained from the H_2O_2–MB reaction depending on the production rate of H_2O_2 in each electrode setup, the percentage of O_2, and water conductivity. A novel work using non-thermal atmospheric plasma in the degradation of dye wastewater assisted by the reverse osmosis process through interfacial mass transfer enhancement was proposed by Chen *et al.*,[40] enhancing the mass transfer of methylene blue in the falling film reactor. The energy yield also increased 1.44 times with the pretreatment of reverse osmosis compared with traditional non-thermal plasma. However, the effects of experimental conditions on MB removal by plasma–liquid interaction (PLI) have not been analyzed comprehensively. Therefore, there is a need for further investigation of the effects of input parameters and optimal conditions for MB removal by NTP treatment. Specifically, they are the MB concentration, reaction time, swirling rate, and the distance between the plasma source and the liquid surface. This research explores the application of a cold Ar plasma jet operating under atmospheric conditions for the removal of MB through plasma–liquid interaction (PLI). This non-thermal plasma approach, implemented on a home-built system, demonstrates impressive MB degradation efficiency, achieving over 80% removal within 30 minutes of treatment. This corresponds to a notable energy efficiency of 55 mg MB per kW per h for an initial MB concentration of 10 mg L^{-1}. To gain a thorough understanding and optimize this treatment process, a comprehensive analysis of the key input parameters for MB removal by PLI was conducted using both experimental investigations and mathematical modelling.

2 Experimental

2.1 Chemicals

Methylene blue trihydrate (Xilong Scientific, $C_{16}H_{18}ClN_3S\cdot 3H_2O$, CAS: 7220-79-3, China) with an assay of 98.5% was dissolved in pure water (distilled water) to create artificial dye wastewater. The dye wastewater with an MB concentration ranging from 5 to 20 mg L^{-1} was used in the experiments. Argon (Ar) gas, used to generate the plasma jet, was supplied from a gas tank with a purity of 99.95%. In the case of aerating the MB solution, either O_2 gas with a purity of 99.99% or air supplied from the atmosphere by a gas pump was used.

2.2 Plasma liquid interaction for MB removal

The experimental schematic of the PLI for MB removal is depicted in Fig. 1. The Ar plasma jet was generated using a gliding configuration,[41] as shown in Fig. 1(a). Two metal electrodes were fixed and placed inside a dielectric funnel with an inner diameter of 4.5 mm for the nozzle exit. The plasma jet was driven by a 50 Hz AC voltage with an amplitude of 2 kV and an Ar flow rate ranging from 2 to 5 L min^{-1}, in which the Ar flow was controlled by applying a ball flow meter. Fig. 1(b) and (c) shows that the images of the plasma jet were generated under an Ar flow rate of 3.5 L min^{-1}. To determine the discharge power of the plasma jet, voltage and current during plasma discharge were measured using a high voltage probe (Pintek, HVP-15HF, China) and a current monitor (Pearson model 410), respectively. These electrical waveforms were recorded using a digital oscilloscope (Tektronix, TDS 2012B, USA); the data were used to estimate plasma discharge power (P) by integrating voltage and current[42] as follows:

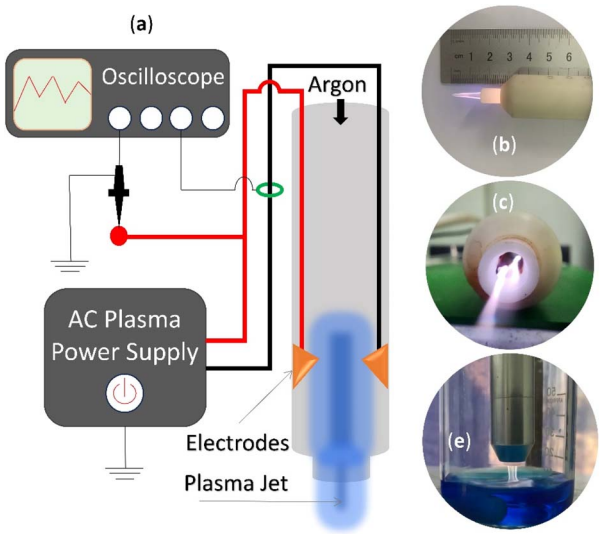

Fig. 1 (a) Schematic of the experimental setup for Ar plasma jet generation, (b) side view of the plasma jet, (c) bottom view of the plasma jet, and (d) Ar plasma jet interacting with MB solution.

$$\text{Discharge power, } P_{\text{avg}}\ (\text{W}) = \frac{1}{T}\int_0^T v(t)\ i(t)\mathrm{d}t. \qquad (1)$$

PLI for MB removal efficiency was performed by the plasma jet source located at the center of a glass beaker (50 mL) that contained 10 mL of MB solution, as shown in Fig. 1(d). Herein, the distance (d) between the nozzle exit and the solution surface was adjusted by applying a lab jack stand table lift; in this study, d was fixed ranging from 5 mm to 15 mm. MB removal by PLI was examined under variation of stirring solution, the distance, interaction time (time treatment), initial MB concentration and Ar flow rate. To evaluate these factors in the treatment, the removal efficiency of MB was calculated by applying eqn (2), in which the MB concentration was measured by the solution absorbance with a 665 nm light source, which was conducted using a UV-Vis (Thermo Scientific, Evolution 350 UV-Vis). The concentrations were estimated through the absorbance calibration curve of standard solutions; the standard MB concentrations ranged from 0 to 20 mg L^{-1}, and the R^2 of the calibration curve was 0.999. Under each experimental condition, the MB concentrations were measured at least three times, and their mean values were used. The absorbance of the MB solutions was measured to two decimals (0.01 scale, corresponding to 0.05 mg L^{-1}), resulting in an error in the MB removal efficiency in the 1.0% range in the experiment.

$$\text{Removal efficiency, } R\ (\%) = \left(1 - \frac{C_{\text{treated}}}{C_{\text{initial}}}\right) \times 100\%. \qquad (2)$$

2.3 Infrared spectroscopy analysis and model for optimizing processes

Infrared spectroscopy analysis of the treated MB solution was carried out by applying a Fourier Transform Infrared Spectrophotometer (FTIR, PerkinElmer, MIR/NIR Frontier). The samples for FTIR analysis were prepared with 2 μL of solution impregnated into 0.1 g KBr; then, the impregnated KBr was compressed into a pellet using the FTIR sample preparation tool. Subsequently, the pellets were used to measure infrared spectra ranging from 400 to 4000 cm^{-1} with a scan number of 20 and a resolution of 4 cm^{-1}.

The removal of MB by PLI processing is complicated and depends on the plasma operating parameters and configuration of the plasma system, *e.g.*, treatment time, initial MB concentration, Ar flow rate, stirring solution, and distance between the plasma jet source and liquid surface. To facilitate the evaluation of these factors on MB removal efficiency by PLI processing, a model with these factors as input variables was used to predict MB removal efficiency. Design-Expert software (version 12) with Box–Behnken design was used to determine and evaluate compatible models. Consequently, the magnitude of the effect of these factors can be represented by the model's coefficients, suggesting optimized conditions and the design of a large-scale PLI system for MB removal.

3 Results and discussion

3.1 Physical properties of the Ar plasma jet

3.1.1. Electrical analysis of plasma discharge. A source of a cold plasma jet using a gliding arc configuration was driven by a 50 Hz pulse voltage supply, as shown in Fig. 2(a). The power supply generated a sinusoidal-like voltage waveform in the no-load mode, where the plasma jet reactor was not connected to a high-voltage line. However, there were significant changes in the voltage waveform during plasma jet production, both in loading mode and interacting mode, *i.e.*, the waveform transitioned from sinusoidal-like to pulsed waveforms. The behavior of the voltage waveform during gliding arc plasma operation was also reported by Matyakubov *et al.*[43] Fig. 2(b) shows that the current discharges exhibited negligible changes between the load and interaction modes. This phenomenon can be explained by the fact that the MB solution behaves similarly to a dielectric surface. Therefore, the floating ground electrode of the MB solution was weak, resulting in insignificant changes in the current discharge waveform.[44] Consequently, the electrical properties of the plasma jet remained stable and consistent during plasma treatment. To support this statement, the evolution of the discharge power is plotted, as depicted in Fig. 2(c), indicating that the discharge power changed negligibly during plasma treatment with a discharge power of approximately 2.9 W.

3.1.2. Optical emission spectra of the plasma jet. The optical emission spectra of the Ar plasma jet during interaction with an ambient atmosphere or MB solution were analyzed in wavelengths ranging from 200 to 650 nm, as shown in Fig. 3. These spectra were recorded by applying an optical emission spectrometer (Ocean Optics, Maya 2000 Pro, USA) with the angle of the center axes between the optical fiber tip and the plasma jet being approximately 70°.

Fig. 3(a) illustrates that typical spectra are similar to those of Ar plasma interacting with the ambient atmosphere or MB solution (10 mg L^{-1}). Particularly, the spectra consisted of

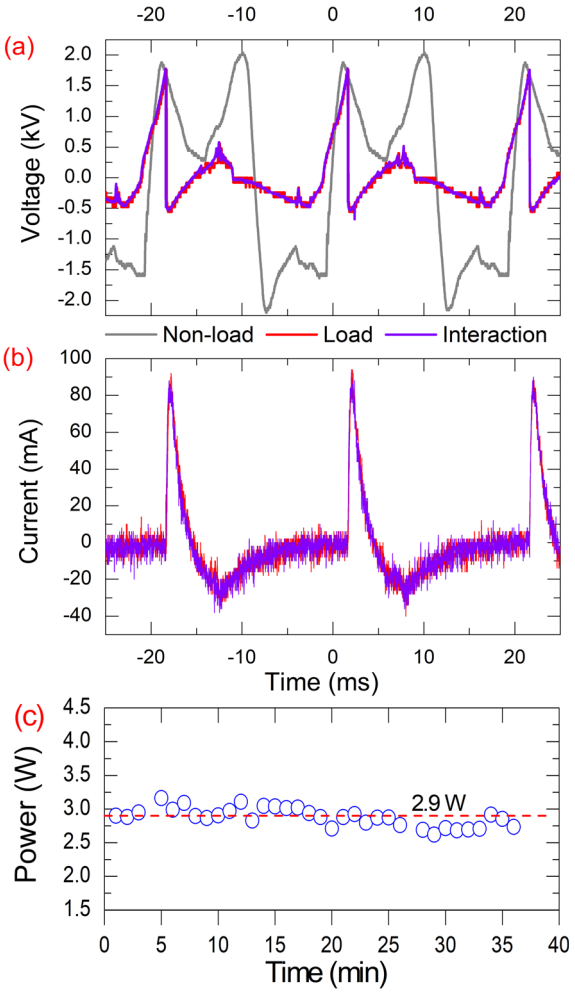

Fig. 2 Typical voltage and current of the plasma jet: (a) voltage waveforms, (b) current discharge, and (c) discharge power (Ar flow rate = 3.5 L min^{-1}).

strong lines of nitrogen in the second positive system ($C^3\Pi_u \rightarrow B^3\Pi_g$) and N_2^+ in the first negative system ($B^2\Sigma_u^+ \rightarrow X^2\Sigma_g^+$), NO emission lines in the range of 200–280 nm ($A^2\Sigma^+ \rightarrow X^2\Pi$), and Ar emissions were presented in the zoom in the spectra in a wavelength ranging from 545 to 615 nm, as shown in Fig. 3(c). Furthermore, in the previous report, Ar emission was unclearly identified in the range of 545–615 nm with an Ar plasma jet generated by the dielectric barrier discharge (DBD).[45] OH peaks overlap with N_2 peaks at 296 and 308 nm. Emissions of Ar in the range 700–850 nm and O at 777 nm are also observed with the Ar plasma jet.[38,45] In comparison, emission intensities under the Ar plasma jet interacted with the ambient atmosphere or MB solution, and the intensity of all lines decreased when the Ar plasma jet interacted with the MB solution. Fig. 3(b) illustrates that the group peaks of N_2 at 380 nm are observed for both spectra; consequently, the vibrational temperature can be determined by the heads of the N_2 bands in the 380 nm region using a temperature calculation tool of the Spectrum Analyzer (version 1.97).[46] Consequently, the vibrational temperature of the Ar plasma jet was 1423 ± 26 K and 1392 ± 15 K (average of three spectra) for interaction with the ambient atmosphere and the MB solution, respectively. The analysis of the optical emission spectra indicated that the Ar plasma jet consisted of several reactive species, such as photons, energetic electrons, ions, and excited species, such as O, O_2^-, OH, Ar*, Ar^+, Ar^m (metastable Ar), N_2^*, and N_2^+. The vibrational temperature of N_2 in the Ar plasma jet was around 1400 K, while the temperature of the Ar plasma jet was not larger than 313 K (≤40 °C; plasma jet temperature).

3.2 Effects of processing parameters on MB removal

Chemical reactions by a PLI process can occur from the interface to the inside bulk liquid,[32] *i.e.* plasma interacts with the surface liquid and results directly in chemical reactions in the thin layer of the interface; consequently, reactive chemical species and other chemical products are formed. Since there are high concentrations in the interface, these chemicals diffuse into the bulk liquid solution and initiate reactions. In the opposite direction, owing to the consumption of chemical reactants in the interface, the concentration of the reactants in the bulk liquid is higher than that in the interface, consequently diffusing the reactants from the bulk solution to the interface to sustain the chemical reactions. Based on the behavior of PLI, the removal of MB inside the solution depends on the stirring solution, initial MB concentration, interaction time, gas injection, flow rate of plasma gas, and distance from the exit nozzle to the surface solution. Consequently, in this section, the removal efficiency of MB as a function of these input parameters is examined and discussed.

3.2.1. Effects of stirring the solution. Fig. 4 illustrates the effect of stirring the solution on the removal efficiency of MB. The results indicate that the MB removal efficiency increases as the stirring speed increases from 50 to 250 rpm. The interaction area between the plasma jet and the liquid is smaller than the liquid surface area, as shown in Fig. 1(d). Nevertheless, the MB concentration decreases with time owing to the PLI. This reduction results from the diffusion of reactants from the bulk liquid into the interaction area and reactive species generated by PLI diffuse from the interaction area into the bulk liquid. Consequently, chemical reactions facilitate MB removal. Stirring enhances the diffusion of chemicals, as well as O_2 and N_2, in the MB solution during PLI, thus improving the removal process. Based on this behavior of MB removal by PLI, stirring the solution increases the MB removal efficiency. However, stirring beyond the stirring range can result in a turbulent liquid state, reducing the MB removal efficiency owing to a decrease in the PLI area.

3.2.2. Effects of concentration and interaction time. The dependence of MB removal efficiency on the initial MB concentration and interaction time was examined under varying concentrations from 5 to 20 mg L^{-1} conjugated with an interaction time of 10–50 min, as shown in Fig. 5. This figure indicates that removal efficiency increased with the interaction time. In contrast, it decreased with an increase in concentration from 5 to 20 mg L^{-1}. An increase in MB removal efficiency resulted from more oxidants being produced owing to the

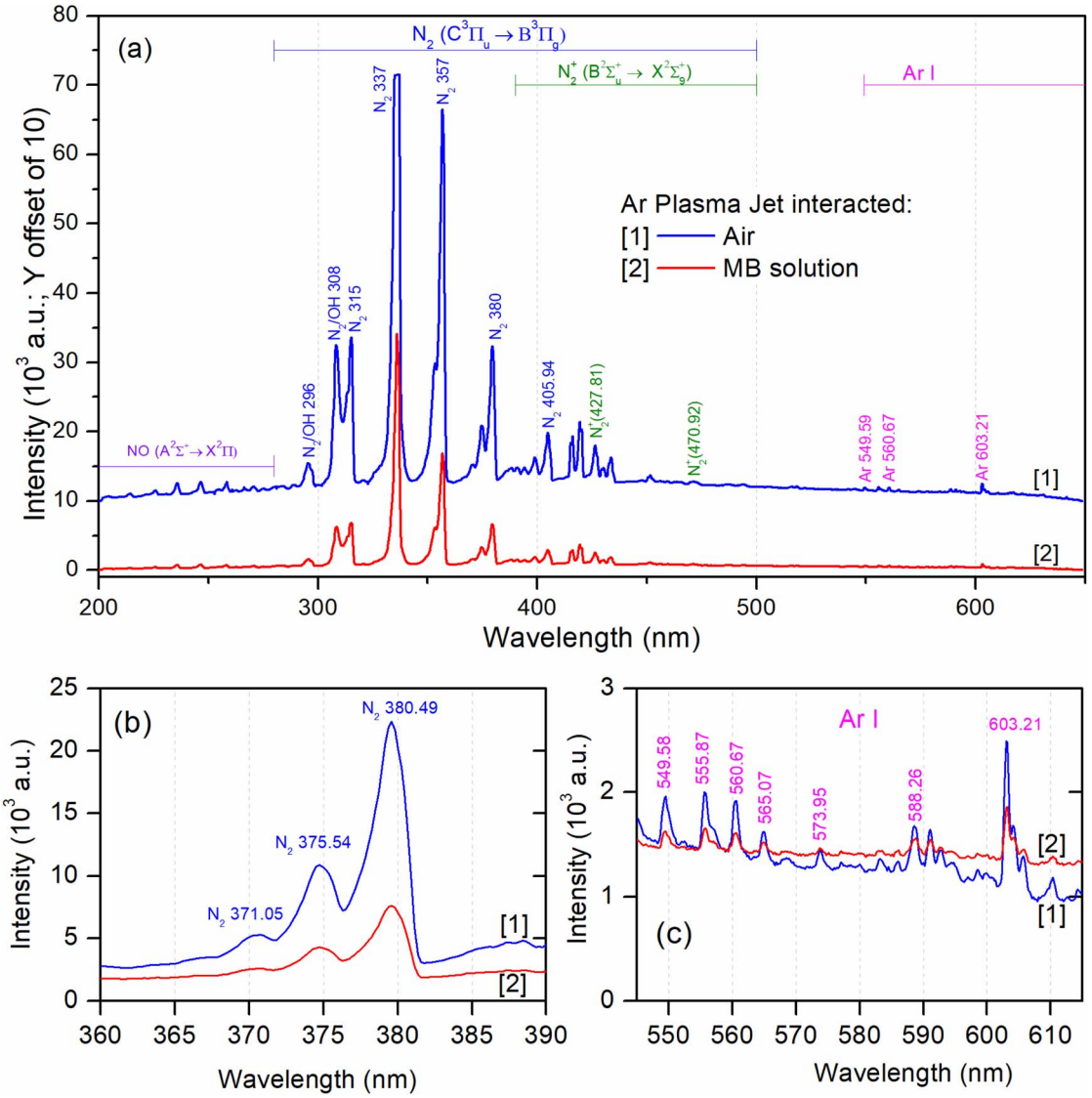

Fig. 3 Optical emission spectra of (a) Ar plasma jet interacted atmosphere [1] and MB solution (PLI) [2], and zoom in with wavelength ranges of 360–390 nm (b) and 545–615 nm (c) (Ar flow rate = 3.5 L min^{-1}; the angle of center axes between the optical fiber tip and plasma jet is approximately 70°; non-stirring solution; acquired mode: average of 10 waveforms).

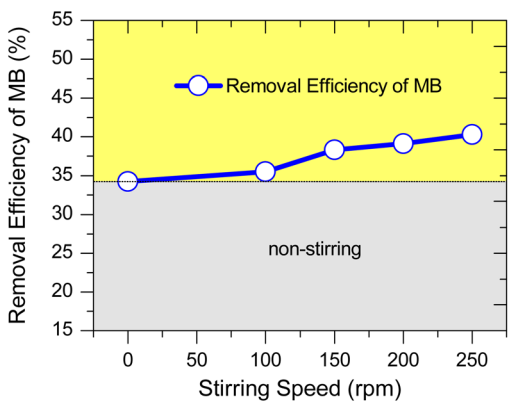

Fig. 4 Effect of stirring solution on the MB removal efficiency (d = 10 mm; initial MB concentration = 10 mg L^{-1}; interaction time = 10 min).

longer interaction time. Huang *et al.*[47] measured the concentration of oxidants during MB solution treatment with plasma. They indicated that the concentration of oxidants increased significantly with treatment time from 0 to 40 min and that high concentrations of oxidants led to high MB degradation. The tendency of the initial MB concentration effect on the removal efficiency of MB is linear with increasing amounts of MB in the feed. Interestingly, with interaction time ≥ 40 min, the removal efficiency slightly depended on concentration, *i.e.*, almost removal efficiency of at least 95% under those conditions. In summary, the removal efficiency strongly depends on the initial MB concentration and treatment time.

3.2.3. Effects of distance and Ar flow rate on MB removal. The physical properties of the plasma jet strongly depend on the gas flow rate and distance from the nozzle exit,[48] such as the temperature of the plasma jet,[49] current emissions of the

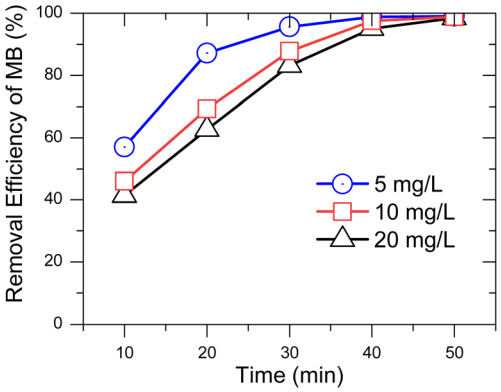

Fig. 5 Effect of initial MB concentration and interaction time on the MB removal efficiency (d = 10 mm; Ar flow rate = 3.5 L min^{-1}; stirring speed = 150 rpm).

plasma jet,[44] and length of the plasma jet,[42] suggesting that PLI for MB removal depends on the Ar flow rate and distance from the exit nozzle to the surface solution. Fig. 6 illustrates the removal efficiency of MB as a function of the Ar flow rate and the distance from the nozzle exit. The results show that removal efficiency decreases as the distance increases from 10 to 20 mm, while it increases as the Ar flow rate increases from 2.5 to 4.5 L min^{-1}. The decrease in efficiency with distance can be explained by a decrease in the velocity, charge and electron density of the plasma bullet at a longer distance from the nozzle exit. Wu *et al.*[50] examined the dependence of plasma bullet velocity on the distance from the nozzle exit for the He plasma jet; the results showed that the velocity of the plasma bullet linearly decreased as the distance increased from 10 to 80 mm. There is a significant decrease in the intensity of the optical emission of species in a long-distance plasma plume, such as excited He, N_2, N_2^+, O, and OH species.[51] Moreover, Oh *et al.*[52] demonstrated that the total net charge and density (absolute value) of the He plasma bullet decreased with distance. In the case of the flow rate, the increase in the removal efficiency of MB with a higher flow rate resulted from the longer plasma with an increased Ar gas velocity. This can be explained by the fact that with a high gas velocity, more energetic electrons and reactivated species entered the interface,[51] resulting in more MB conversion.

3.2.4. Effects of injecting gases. There are more reactive oxygen species that can be formed during the plasma jet interaction with oxygen molecules;[49] consequently, this results in more MB molecules undergoing oxidation. In this section, the effect of air/O_2 aeration inside the solution on MB removal efficiency was examined as the interaction time increased from 10 to 50 min. The results are illustrated in Fig. 7. This figure shows that the MB removal efficiency with air/O_2 aeration was higher than that with no aeration. However, the effectiveness of aeration decreased with interaction time, and the gas order is none < air < O_2. In other words, with time treatment ≥ 40 min, there is no need for gas aeration. The increase in MB removal efficiency due to gas aeration can be explained by gas bubbles created inside the MB solution. During the PLI process, more oxygen species are formed on the interface of the bubbles; the greater effectiveness of O_2 aeration compared to air aeration also supports this hypothesis: O_2 flow consists of 99.99% oxygen, while air flow has only 21% oxygen. In this experiment, the MB solution was artificial dye waste, with MB dissolved in pure water. Consequently, the MB solution became saturated with O_2 through the diffusion of O_2 in the atmosphere into the MB solution when it was exposed to the surrounding ambiance. This provides a reasonable explanation for a slight increase from 2 to 5% in removal efficiency with air/O_2 aeration. Overall, the plasma treatment still achieved high removal efficiencies of MB without air/O_2 aeration; regarding the economic efficiency of the process, air/O_2 aeration is not necessary with the artificial dye waste solution.

3.3 Optimizing input parameters for processing

As observed in the results above, the removal of MB by PLI treatment has a complicated dependence on input parameters, such as stirring (S), interaction time (T), distance between the liquid surface and the plasma jet source (D), initial MB concentration (C), and Ar flow rate (F). To evaluate the variation in these factors in the removal efficiency of MB by the PLI

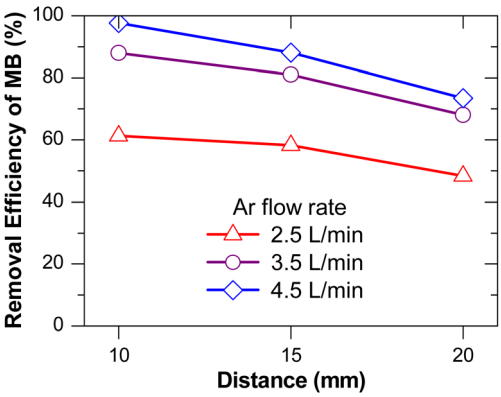

Fig. 6 Effect of distance conjugated with Ar flow rate on the MB removal efficiency (initial MB concentration = 10 mg L^{-1}; interactive time = 30 min; stirring speed = 150 rpm).

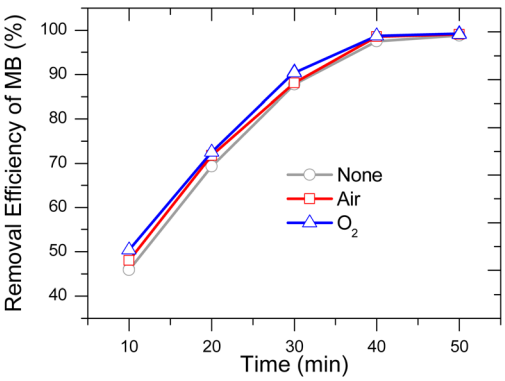

Fig. 7 Effect of air/O_2 aeration into the MB solution on the MB removal efficiency (d = 10 mm; initial MB concentration = 10 mg L^{-1}; stirring speed = 150 rpm; flow rate of air/O_2 = 1.6 L min^{-1}).

Table 1 Variables and their properties for the quadratic model

Name	Code	Units	Type	Changes	Std. dev.	Low	High
Stirring speed	S	rpm	Independent variables	Easy		0	200
Distance between the nozzle exit and liquid surface	D	cm		Easy		1	2
Interaction time	T	min		Easy		10	50
Initial MB concentration	C	mg L^{-1}		Easy		5	15
Ar flow	F	L min^{-1}		Easy		2.5	4.5
Removal efficiency	R	%	Observed variable		5.8	29.3	99.8

treatment, a quadratic model of these factors (independent variables) for predicting MB removal efficiency (the observed variable) was carried out using a Box–Behnken design. In brief, the independent variables were the five factors listed above, with MB removal efficiency as the observed variable, as shown in Table 1. Estimating coefficients and analysing the quadratic model were carried out using Design-Expert software (version 12). The input experimental data are presented in Table S1 in the ESI.† Furthermore, the results of the ANOVA analysis for the quadratic model are presented in the ESI.†

Consequently, the removal efficiency of MB by PLI can be estimated using the coded quadratic equation (eqn (3)). The quadratic equation is significant in describing the variation in MB removal efficiency by PLI treatment. In fact, the correlative experimental data compared with the predicted data by the model are presented in Fig. 8. The fit of the model resulted in $R^2 = 0.9493$, adjusted $R^2 = 0.9336$ and predicted $R^2 = 0.9099$. This means that 90% of the variation in MB removal efficiency can be explained by these independent variables using eqn (3). The remaining variation in MB removal efficiency (~10%) can be accounted for by other factors that are not included in the model, such as varying discharge power (see Fig. 2(c)), ambient temperature, and atmospheric humidity.

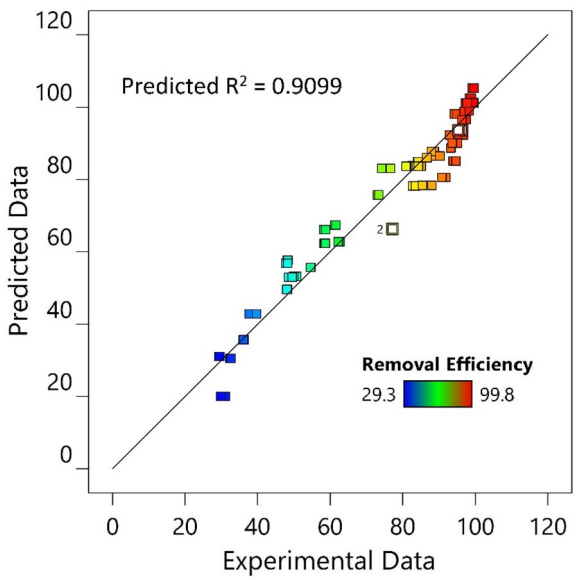

Fig. 8 Correlative experimental data with the predicted data using the quadratic model.

$$R = 83.61 + 5.88S - 7.84D + 27.49T - 9.58C + 12.01F + 7.22SD + 2.33ST + 5.18SC - 0.7250SF + 3.48DT - 2.28DC - 2.58DF + 6.06TC - 2.76TF + 1.72CF - 3.84S^2 - 1.24D^2 - 13.06T^2 + 3.58C^2 - 8.31F^2, \quad (3)$$

where S, D, T, C, and F are coded, representing the above independent variables, with values in the range of $[-1, 1]$. A value of -1 represents the low level of the variables, while +1 represents the high level, as shown in Table 1.

Since the linear equation (eqn (4)) for the process has a predicted R^2 of 0.7875, with only a small difference (0.1224) compared to the quadratic equation (predicted $R^2 = 0.9099$), the first-order coefficients of the model were used for a comparison between these factors affecting the MB removal efficiency. Consequently, according to these coefficients, stirring (S), interaction time (T, time treatment), and Ar flow rate (F) factors have positive effects. In contrast, the distance between the nozzle exit and the liquid surface (D) and the initial concentration (C) negatively affect MB removal efficiency. Using the standard unit of S, D, T, C, and F as 100 rpm, 0.5 cm, 20 min, 5 mg L^{-1}, and 1 L min^{-1}, respectively, the order of the effective factors on MB removal efficiency was $T > F > C > D > S$ (27.49 > 12.01 > 9.58 > 7.84 > 5.88). In other words, the three plasma operating parameters are interaction time, Ar flow rate, and initial MB concentration, which strongly affect the MB removal efficiency. For the plasma system configuration factors, such as the distance and stirring of the solution, MB removal efficiency can potentially be enhanced, *i.e.*, stirring at 150 rpm and a distance of 10 mm are recommended settings. In summary, the quadratic model analysis of the five factors confirmed the impact of these factors on the MB removal efficiency. Almost all changes in MB removal efficiency can be explained by the five factors; specifically, at least 90% of MB removal efficiency was described using eqn (3). Interestingly, based on the comparison of the first-order coefficients of the model, the magnitude and tendency of each factor's effect can be easily determined and evaluated for MB removal efficiency by PLI treatment.

$$R = 75.0977 + 5.88S - 7.84D + 27.49T - 9.58C + 12.01F. \quad (4)$$

In summary, after 50 min of the PLI treatment, about 99.0% of the initial MB (≤20 mg L^{-1}) can be degraded, with an energy efficiency of 82.76 mg MB per kW per h or an energy consumption of 241.67 kW h m^{-3}. Compared with MB degradation by the flat DBD,[53] the energy efficiency of the Ar plasma

jet is higher than that of the flat DBD, which was obtained at 46.7 mg MB per kW per h. Pereira *et al.*[54] treated the removal of 5 mg MB per L (volume: 50 mL) using a TiO_2 P25 photocatalyst with a UV source at 365 nm and a power consumption of 11 W within 30 min of exposing the sample to UV radiation. Consequently, the energy efficiency of the photocatalytic method is estimated to be 45.5 mg MB per kW per h (110 kW h m^{-3}). Here, it should be noted that when the photocatalytic process uses sunlight for treatment, no electric energy is consumed. The decomposition of methylene blue by electrochemical oxidation was reported by Teng *et al.*[55] The energy consumption is 21.35 kW h m^{-3} with an initial MB of 10 mg L^{-1}, corresponding to an energy efficiency of 468 mg MB per kW per h. Compared to the above methods for MB decomposition, PLI has comparable energy efficiency or energy consumption; however, achieving a large area of PLI using a plasma jet configuration is a challenge.

3.4 Reaction underlying MB removal by PLI treatment

The destruction of MB by the Ar plasma jet process can be divided into three zones, as shown in Table 2. First, there is the discharge zone, where electron impact reactions occur by (R1)–(R3) reactions to form energetic electrons, excited Ar atoms, and metastable Ar.[38] Second, in the interaction stage, the Ar plasma exits the tube orifice into the surrounding ambient air (gas phase) and then hits the liquid surface (mixture phase). During the propagation of the Ar plasma jet, the jet interacts with the surrounding ambient air, consisting mainly of N_2, O_2, and H_2O_{gas} and a small amount of CO_2 (a few hundred ppm). Therefore, with the flow of the Ar plasma jet containing reactive species, their species interacted with the ground state molecules of the surrounding environment to form other products, as shown in (R4)–(R14).[32] The optical emission spectrum analysis confirmed that O, O_2^-, OH, Ar*, Ar^+, Ar^m, N_2^*, and N_2^+ are formed. Furthermore, O_3 and NO_x are detected as products during the interaction of the Ar plasma jet (DBD) with the surrounding ambient air.[45] At the interface, reactions are added by the presence of MB and more H_2O in the liquid phase, specifically dissolved chemicals from the gas phase into the bulk or reaction with H_2O (R15) and (R16). In the case of MB molecules on the liquid surface, there can be a collision between MB molecules and the reactive species generated by the Ar plasma to break down MB molecules into light molecules and short carbon chains (R17). The treated MB solution was analyzed by FTIR and compared with the literature survey to determine possible reactions for breaking MB and the bulk liquid stage.

Fig. 9 shows the FTIR spectra of the original MB solution and MB solutions treated with plasma for 10, 30, and 50 minutes. The broad bands around 3460 cm^{-1} in the untreated MB sample correspond to O–H stretching vibrations from water in the sample.[56,57] However, it overlapped with the $-NH_2$ peak (3415 cm^{-1}) in the treated MB samples, indicating that the N–CH_3 bond was dissociated to form $-NH_2$ by energetic electrons and oxidants ($^{\bullet}OH$, O_3).[47] The group peaks in the range of 2900–3000 cm^{-1} were assigned to C–H stretching vibrations from –CH_3 methyl groups and CH in the aromatic ring for all typical samples. Group peaks from 1390 to 1620 were attributed to the

Table 2 Possible reactions during PLI for MB removal[a]

Region/phase		Reaction	
Discharge zone (gas phase)		$Ar + e \rightarrow Ar^* + e$	R1
		$Ar + e \rightarrow Ar^+ + e + e$	R2
		$Ar + e \rightarrow Ar^m + e$	R3
Interaction	Air (gas phase)	$O_2 + e \rightarrow O_2^-$	R4
		$O_2 + e/M \rightarrow 2O + e/M$	R5
		$O + O_2 + e/M \rightarrow O_3 + e/M$	R6
		$N_2 + e/M \rightarrow N_2^* + e/M$	R7
		$N_2 + e/M \rightarrow N_2^+ + e + e/M$	R8
		$O_2 + N_2 + e/M \rightarrow 2NO + e/M$	R9
		$O_2 + \frac{1}{2}N_2 + e/M \rightarrow NO_2 + e/M$	R10
		$O + NO + e/M \rightarrow NO_2 + e/M$	R11
		$H_2O + e/M \rightarrow H_2O^* + e/M$	R12
		$H_2O + e/M \rightarrow OH + H + e/M$	R13
		$H_2O + O + e/M \rightarrow OH + OH + e/M$	R14
	Interface (mixture phase)	$H_2O + O + e/M \rightarrow H_2O_2 + e/M$	R15
		$2NO_2 + H_2O \rightarrow 2H^+ + NO_3^- + NO_2^-$	R16
		$(CH_3)_2N–R^+–NH_2 + e/M + O/OH/O_3 \rightarrow H_2N–RO–NH_2 + HCHO + products$	R17
Bulk liquid (liquid phase)		$(CH_3)_2N–R^+–N(CH_3)_2 + OH/O_3 \rightarrow H_2N–RO–NH_2 + HCHO + products$	R18
		$(CH_3)_2N–RO–N(CH_3)_2 + OH/O_3 \rightarrow products + C_7H_5NS + single\ ring\ structure$	R19
		$Products/C_7H_5NS/single\ ring\ structure + OH/O_3 \rightarrow NO_3^- + SO_4^{2-} + CO_2 + H_2O + products$	R20

[a] M represents excited molecules, Ar metastable, and ions; $(CH_3)_2N–R^+–N(CH_3)_2$ represents the cation part of the MB structure ($C_{16}H_{18}ClN_3S$).[56]

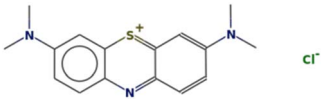

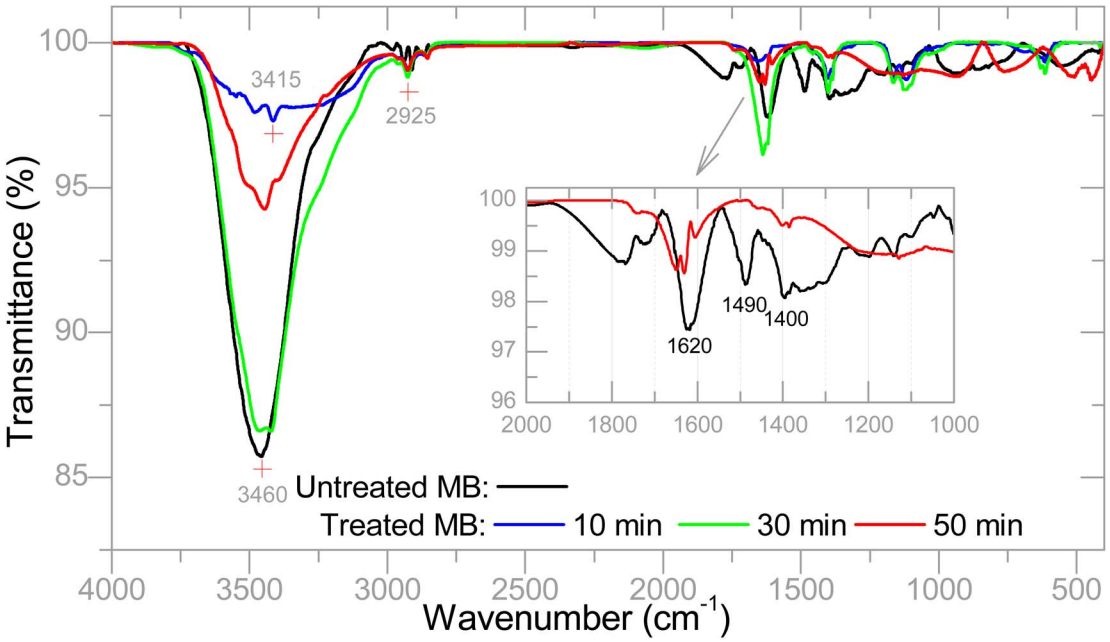

Fig. 9 FTIR spectra of MB and MB treated with plasma with interaction times of 10, 30, and 50 min.

vibrations of aromatic ring structures in MB molecules.[58] A comparison between the original MB and the 50 minute treated MB solution (showing over 90% MB degradation), displayed in the inset figure, reveals a significant decrease in peak intensities. Notably, the peak at 1490 cm^{-1} is absent in the treated MB samples. This demonstrates that plasma treatment led to changes in the aromatic ring structures of MB molecules, breaking chemical bonds to form lighter molecules. For example, benzothiazole (C_7H_5NS) and *N*-(4-nitrophenyl)butanamide can be produced during plasma treatment of the MB solution.[47,59] Furthermore, the pH of the treated solution (measured with pH indicator paper) decreased with treatment time. The pH after 50 min of treatment was in the range of 5–6. This result agreed with a previous report.[47] H_2O, CO_2, $Cl-$, NO_3^-, and SO_4^{2-} were the final products of the MB solution treated with air plasma. Overall, the reactions decomposing MB into smaller molecules using atmospheric-pressure DBD plasma, as introduced by Huang *et al.*,[47] are suitable for removing MB by the Ar plasma jet, as shown in (R18)–(R20), which is adapted from this reference.

4 Conclusions

The removal of MB in the artificial wastewater was achieved through a PLI, which was created by the cold Ar plasma jet interacting with the solution. The PLI for MB removal strongly depended on the input parameters. Specifically, the MB removal efficiency increased with a higher Ar flow rate, longer interaction time (treatment time), and stirring of the MB solution. However, increasing the distance from the nozzle exit to the liquid surface and higher initial MB concentrations led to a decrease in MB removal efficiency. The effects of the input parameters on MB removal efficiency were complicated. To compare the magnitude of the effect of the above factors, MB removal efficiency was modeled as a quadratic equation of these factors, and the coefficients of the model were estimated with a Box–Behnken design and Design-Expert software. The model showed good agreement in predicting MB removal efficiency with the input parameters. Moreover, the first-order coefficients represented the magnitude of each factor's effect in the following order: treatment time > Ar flow rate > initial MB concentration > distance from nozzle exit to liquid surface > stirring solution. This result is meaningful for optimizing the plasma configuration and operating parameters for MB removal through PLI. For instance, to reduce treatment time while achieving high MB removal efficiency, the plasma system requires a large plasma exposure area.

Data availability

The data supporting this article have been included as part of the ESI.† The remaining data are available from the authors upon request.

Author contributions

D. T. V. was involved in investigation and writing-original draft. N. T. D. was involved in investigation, methodology, writing-review & editing, and supervision. T. H. T. L., D. T. N. and L. T. P. were involved in investigation. H. T. D. was involved in investigation and resources. Y. S. M. was involved writing-review & editing, resources, and supervision. D. B. N. was involved in conceptualization, methodology, investigation, resources, writing-original draft, writing-review & editing, and supervision.

Conflicts of interest

The authors declare no financial or commercial conflict of interest.

Acknowledgements

This research was supported in part by the Kurita Asia Research Grant (23Pvn046) provided by Kurita Water and Environment Foundation, Vietnam, and by the National Research Foundation of Korea (NRF) grant funded by the Korea government (MSIT) (No. RS-2024-00405278).

Notes and references

1 N. Roy, N. T., P. Paira and R. Chakrabarty, *RSC Adv.*, 2025, **15**, 3008–3025.
2 A. P. Provin, A. Medeiros d'Alva, A. R. d. A. Dutra, J. B. S. O. d. A. Guerra and A. L. V. Cubas, *J. Cleaner Prod.*, 2024, **470**, 143352.
3 N. T. Dinh, L. N. H. Vo, N. T. T. Tran, T. D. Phan and D. B. Nguyen, *RSC Adv.*, 2021, **11**, 20292–20302.
4 P. O. Oladoye, T. O. Ajiboye, E. O. Omotola and O. J. Oyewola, *Results Eng.*, 2022, **16**, 100678.
5 J. Cheng, C. Zhan, J. Wu, Z. Cui, J. Si, Q. Wang, X. Peng and L.-S. Turng, *ACS Omega*, 2020, **5**, 5389–5400.
6 K. F. Kayani, *RSC Adv.*, 2024, **14**, 31777–31796.
7 S. W. Goh, Q. H. Ng, S. K. E. A. Rahim, S. C. Low, P. Y. Hoo, R. Y. Z. Yeo, T. L. Chew and Z. A. Jawad, *J. Water Proc. Eng.*, 2025, **70**, 106993.
8 S. Samsami, M. Mohamadizaniani, M.-H. Sarrafzadeh, E. R. Rene and M. Firoozbahr, *Process Saf. Environ. Prot.*, 2020, **143**, 138–163.
9 Q. Lu, J. Li, B. Wang, J. Yu, X. Ma, L. Cui and Y. Feng, *Plasma Processes Polym.*, 2022, **19**, 2100172.
10 R. S. Dhamorikar, V. G. Lade, P. V. Kewalramani and A. B. Bindwal, *J. Ind. Eng. Chem.*, 2024, **138**, 104–122.
11 M. S. Sheikh, M. M. Rahman, M. S. Rahman, K. Yildirim and M. Maniruzzaman, *J. Ind. Eng. Chem.*, 2023, **128**, 196–208.
12 J.-C. Lee, H.-J. Kim, H.-W. Kim and H. Lim, *J. Ind. Eng. Chem.*, 2021, **98**, 383–388.
13 G. Cao, R. Wang, Y. Ju, B. Jing, X. Duan, Z. Ao, J. Jiang, F. Li and S.-H. Ho, *Water Res.*, 2021, **206**, 117741.
14 M. Behera, J. Nayak, S. Banerjee, S. Chakrabortty and S. K. Tripathy, *J. Environ. Chem. Eng.*, 2021, **9**, 105277.
15 K. G. Akpomie and J. Conradie, *Ecotoxicol. Environ. Saf.*, 2020, **201**, 110825.
16 V. Katheresan, J. Kansedo and S. Y. Lau, *J. Environ. Chem. Eng.*, 2018, **6**, 4676–4697.
17 A.-J. Wang, H.-C. Wang, H.-Y. Cheng, B. Liang, W.-Z. Liu, J.-L. Han, B. Zhang and S.-S. Wang, *Environ. Sci. Ecotechnol.*, 2020, **3**, 100050.
18 X. Wang, J. Xia, S. Ding, S. Zhang, M. Li, Z. Shang, J. Lu and J. Ding, *Ecotoxicol. Environ. Saf.*, 2020, **203**, 110945.
19 S. S. Ali, R. Al-Tohamy, J. Sun, J. Wu and L. Huizi, *Fuel*, 2019, **236**, 1128–1145.
20 S. S. Ali, R. Al-Tohamy, R. Xie, M. M. El-Sheekh and J. Sun, *Bioresour. Technol.*, 2020, **313**, 123631.
21 S. S. Ali, J. Sun, E. Koutra, N. El-Zawawy, T. Elsamahy and M. El-Shetehy, *Fuel*, 2021, **285**, 119050.
22 S. S. Ali, R. Al-Tohamy and J. Sun, *Sci. Total Environ.*, 2022, **806**, 150665.
23 N. Morin-Crini, E. Lichtfouse, M. Fourmentin, A. R. L. Ribeiro, C. Noutsopoulos, F. Mapelli, É. Fenyvesi, M. G. A. Vieira, L. A. Picos-Corrales, J. C. Moreno-Pirajᾶn, L. Giraldo, T. Sohajda, M. M. Huq, J. Soltan, G. Torri, M. Magureanu, C. Bradu and G. Crini, *Environ. Chem. Lett.*, 2022, **20**, 1333–1375.
24 L. L. Coria-Oriundo, F. Battaglini and S. A. Wirth, *Ecotoxicol. Environ. Saf.*, 2021, **217**, 112237.
25 R. Al-Tohamy, S. S. Ali, F. Li, K. M. Okasha, Y. A.-G. Mahmoud, T. Elsamahy, H. Jiao, Y. Fu and J. Sun, *Ecotoxicol. Environ. Saf.*, 2022, **231**, 113160.
26 K. N. Pandiyaraj, D. Vasu, A. Raji, R. Ghobeira, P. S. E. Tabaei, N. De Geyter, R. Morent, M. C. Ramkumar, M. Pichumani and R. R. Deshmukh, *J. Ind. Eng. Chem.*, 2023, **122**, 185–199.
27 A. Kumar, N. Škoro, W. Gernjak and N. Puač, *Eur. Phys. J. D*, 2021, **75**, 283.
28 T. N. Kumar, S. Mohapatro and R. R. Dash, *Int. J. Environ. Sci. Technol.*, 2024, **21**, 7819–7836.
29 C. Jiang, C. Qin, M. Guo, J. Huang, D. Yan and X. Dang, *J. Ind. Eng. Chem.*, 2022, **113**, 247–253.
30 A. Kumar, N. Škoro, W. Gernjak, O. Jovanović, A. Petrović, S. Živković, E. C. Lumbaque, M. J. Farré and N. Puač, *Sci. Total Environ.*, 2023, **864**, 161194.
31 L. L. Alves and A. V. Keudell, Foundations of low temperature plasmas and their applications, 2024, **https://iopscience.iop.org/journal/0963-0252/special/0963-0252_focus_issue_Foundations-of-low-temperature-plasmas-and-their-applications**, accessed 05/11/2024.
32 P. J. Bruggeman, M. J. Kushner, B. R. Locke, J. G. E. Gardeniers, W. G. Graham, D. B. Graves, R. C. H. M. Hofman-Caris, D. Maric, J. P. Reid, E. Ceriani, D. F. Rivas, J. E. Foster, S. C. Garrick, Y. Gorbanev, S. Hamaguchi, F. Iza, H. Jablonowski, E. Klimova, J. Kolb, F. Krcma, P. Lukes, Z. Machala, I. Marinov, D. Mariotti, S. M. Thagard, D. Minakata, E. C. Neyts, J. Pawlat, Z. L. Petrovic, R. Pflieger, S. Reuter, D. C. Schram, S. Schröter, M. Shiraiwa, B. Tarabová, P. A. Tsai, J. R. R. Verlet, T. v. Woedtke, K. R. Wilson, K. Yasui and G. Zvereva, *Plasma Sources Sci. Technol.*, 2016, **25**, 053002.
33 R. P. Gott, M. E. Thompson, B. C. Staton, B. M. Williams and K. G. Xu, *IEEE Trans. Plasma Sci.*, 2021, **49**, 2113–2124.
34 Y. Takemura, N. Yamaguchi and T. Hara, *Jpn. J. Appl. Phys.*, 2013, **52**, 056102.
35 M. Radetić and D. Marković, *Plasma Processes Polym.*, 2022, **19**, 2100197.
36 P. J. Bruggeman, A. Bogaerts, J. M. Pouvesle, E. Robert and E. J. Szili, *J. Appl. Phys.*, 2021, **130**, 200401.
37 N. Aloui, J. Pregent, C. Gouze, I. Belgacem and A. Hamdan, *Plasma Chem. Plasma Process.*, 2024, **44**, 1753–1771.

38 N. Aloui, I. Belgacem and A. Hamdan, *Plasma Chem. Plasma Process.*, 2024, **44**, 1971–1989.
39 A. Krosuri, S. Wu, M. A. Bashir and M. Walquist, *J. Water Proc. Eng.*, 2021, **40**, 101926.
40 H. Chen, X. Zhang, C. Shen, Y. Wang, Z. Li, B. Cao and S. Wang, *Chem. Eng. Sci.*, 2023, **282**, 119221.
41 D. H. Tung, B. S. Minh, V. T. Thom, L. T. H. Trang, C. T. Huong and N. T. Tuyen, *Commun. Phys.*, 2016, **24**, 103–108.
42 D. B. Nguyen, Y. S. Mok and W. G. Lee, *IEEE Trans. Plasma Sci.*, 2019, **47**, 4795–4801.
43 N. Matyakubov, D. B. Nguyen, S. Saud and Y. S. Mok, *Ind. Eng. Chem. Res.*, 2022, **61**, 3365–3373.
44 D. B. Nguyen, Q. H. Trinh, M. M. Hossain, W. G. Lee and Y. S. Mok, *IEEE Trans. Plasma Sci.*, 2019, **47**, 2004–2010.
45 D. B. Nguyen, Q. H. Trinh, W. G. Lee and Y. S. Mok, *Plasma Sci. Technol.*, 2019, **21**, 095401.
46 Z. Navrátil, D. Trunec, R. Šmíd and L. Lazar, *Czech J. Phys.*, 2006, **56**, B944–B951.
47 F. Huang, L. Chen, H. Wang and Z. Yan, *Chem. Eng. J.*, 2010, **162**, 250–256.
48 X. Lu, M. Laroussi and V. Puech, *Plasma Sources Sci. Technol.*, 2012, **21**, 034005.
49 D. B. Nguyen, Q. H. Trinh, Y. S. Mok and W. G. Lee, *Plasma Sources Sci. Technol.*, 2020, **29**, 035014.
50 S. Wu, X. Lu and Y. Pan, *Phys. Plasmas*, 2014, **21**, 073509.
51 N. Mericam-Bourdet, M. Laroussi, A. Begum and E. Karakas, *J. Phys. D: Appl. Phys.*, 2009, **42**, 055207.
52 J.-S. Oh, J. L. Walsh and J. W. Bradley, *Plasma Sources Sci. Technol.*, 2012, **21**, 034020.
53 H. K. Kim, G. W. Yang and Y. C. Hong, *Plasma*, 2024, **7**, 767–779.
54 M. d. S. Pereira, R. P. Mendes, G. C. Bellettini, R. M. Benetti, F. Elyseu and A. M. Bernardin, *J. Photochem. Photobiol., A*, 2023, **435**, 114304.
55 X. Teng, J. Li, Z. Wang, Z. Wei, C. Chen, K. Du, C. Zhao, G. Yang and Y. Li, *RSC Adv.*, 2020, **10**, 24712–24720.
56 National Institute of Standards Technology, *NIST Chemistry WebBook*, 2023, DOI: **10.18434/T4D303**.
57 X.-S. Hu, R. Liang and G. Sun, *J. Mater. Chem. A*, 2018, **6**, 17612–17624.
58 Y.-Y. Lau, Y.-S. Wong, T.-T. Teng, N. Morad, M. Rafatullah and S.-A. Ong, *RSC Adv.*, 2015, **5**, 34206–34215.
59 M. A. Adelin, G. Gunawan, M. Nur, A. Haris, D. S. Widodo and L. Suyati, *J. Phys.:Conf. Ser.*, 2020, **1524**, 012079.